Data in brief 25 (2019) 104208

Contents lists available at ScienceDirect

Data in brief

journal homepage: www.elsevier.com/locate/dib

Data Article

Linear, planar and spherical tensor-valued diffusion MRI data by free waveform encoding in healthy brain, water, oil and liquid crystals

Filip Szczepankiewicz [a, b, *], Scott Hoge [a, b], Carl-Fredrik Westin [a, b]

[a] Radiology, Brigham and Women's Hospital, Boston, MA, USA
[b] Harvard Medical School, Boston, MA, USA

ARTICLE INFO

Article history:
Received 27 February 2019
Received in revised form 6 June 2019
Accepted 25 June 2019
Available online 2 July 2019

Keywords:
Diffusion magnetic resonance imaging
Multidimensional diffusion encoding
B-tensor encoding
Free waveform encoding
Human brain in vivo
Water
Oil
Liquid crystal

ABSTRACT

Recently, several biophysical models and signal representations have been proposed for microstructure imaging based on tensor-valued, or multidimensional, diffusion MRI. The acquisition of the necessary data requires non-conventional pulse sequences, and data is therefore not available to the wider diffusion MRI community. To facilitate exploration and development of analysis techniques based on tensor-valued diffusion encoding, we share a comprehensive data set acquired in a healthy human brain. The data encompasses diffusion weighted images using linear, planar and spherical diffusion tensor encoding at multiple b-values and diffusion encoding directions. We also supply data acquired in several phantoms that may support validation. The data is hosted by GitHub: https://github.com/filip-szczepankiewicz/Szczepankiewicz_DIB_2019.

* Corresponding author. Harvard Medical School, Brigham and Women's Hospital, Department of Radiology, 1249 Boylston Street, Boston, MA 02215, USA.
E-mail address: fszczepankiewicz@bwh.harvard.edu (F. Szczepankiewicz).

https://doi.org/10.1016/j.dib.2019.104208

Specifications table

Subject area	Magnetic resonance imaging physics
More specific subject area	Diffusion magnetic resonance imaging
Type of data	Diffusion-weighted signal
How was data acquired	Spin-echo with echo-planar readout with free waveform diffusion encoding on clinical MRI hardware
Data format	Raw anonymized data in DICOM and NIfTI formats with native and complementary metadata
Experimental factors	Signal was diffusion-weighted with linear, planar and spherical b-tensor encoding in healthy human brain, oil, water and hexagonal phase liquid crystal at encoding strength up to 2 ms/μm^2 for 10 to 46 rotations.
Experimental features	Linear and spherical encoding are matched with respect to the diffusion time spectrum along one direction. Encoding tensor shapes, strengths and rotations were distributed over time to minimize effects of drift.
Data source location	Brigham and Women's Hospital, Boston, MA, USA
Data accessibility	Multi-format raw data with corresponding metadata is available at: https://github.com/filip-szczepankiewicz/Szczepankiewicz_DIB_2019

Value of the data

- The data facilities design and testing of analysis techniques that require tensor-valued (or multidimensional) diffusion encoding. This provides value since acquisition of such data currently relies on a custom pulse sequence that is not widely available.
- The data includes repeated sampling of spherical b-tensors for analysis of noise characteristics.
- A subset of the data is matched with respect to the diffusion time spectrum for analysis of models of diffusion time dependency.

1. Data

This dataset contains diffusion weighted magnetic resonance imaging (MRI) data as well as fluid attenuated inversion recovery T_2-weighted morphological images (T_2-FLAIR) and can be found at https://github.com/filip-szczepankiewicz/Szczepankiewicz_DIB_2019. Experiments were performed in a healthy human brain in vivo, water, oil and hexagon phase liquid crystals (Figs. 1 and 2).

Data was exported from the scanner in the native DICOM format and anonymized using DicomCleaner (http://www.pixelmed.com/cleaner.html, access date 2019-02-10). We removed subject identity, replaced all UIDs and hardware and institution ID. All tags described by Newhauser et al. [1] were either removed or overwritten with anonymized variants. The vendor-specific private tags were unaltered. These contain information that is specific to the free waveform (FWF) sequence, such as waveform timing, gradient scaling and balance gradient parameters; necessary to reconstruct the experiment in detail. We also provide FWF-header tools that are capable of extracting this information, available at https://github.com/filip-szczepankiewicz/fwf_header_tools. DICOM images for each subject are stored in folders denoted 'DICOM_zip' in a compressed format (.zip).

Anonymized DICOM images were converted to 4D NIfTI files in a compressed format (.nii.gz), along with b-value (.bval) and encoding direction files (.bvec), using MRIcroGL (v1.0.20180623, https://www.nitrc.org/projects/mricron). These files are stored under folders denoted 'NII' along with corresponding meta data files (.json).

NIfTI images were also prepared to be compatible with the multidimensional diffusion MRI framework [2] available at https://github.com/markus-nilsson/md-dmri. As such, the diffusion-weighted data from each subject or phantom was merged into a single 4D-volume and an appropriate experimental parameter structure (_xps.mat) was constructed. These files are denoted 'FWF_MERGED' and are stored in folders denoted 'MD-dMRI'. In addition to the original in vivo data, we provide a set of data that was corrected for motion and eddy-currents by registering the images to an extrapolated reference [3] using ElastiX [4]. These files are denoted with a suffix '_mc'.

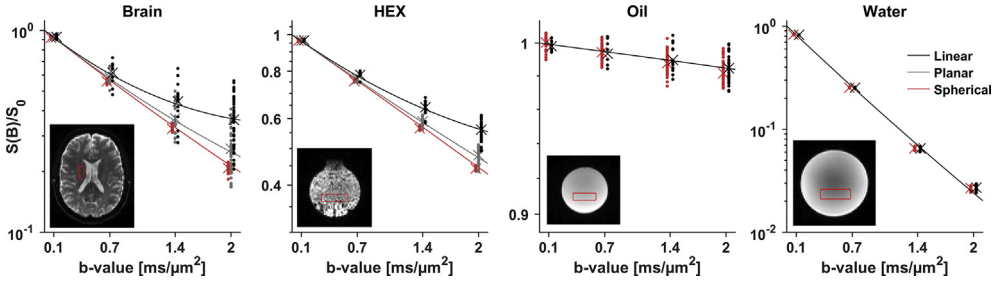

Fig. 1. Signal versus b-value in brain and phantoms that contain HEX, oil or water. The circular markers are individual signal measurements (shifted along b to avoid overlap) and the crosses show the average signal for each combination of b-tensor shape and b-value in the ROIs (red outline in inset plots). The solid lines show the trend of the signal averaged over rotations of all b-tensors with a given b-value and shape, based on the q-space trajectory imaging representation [12]. Note that the scales of the y-axes are different across objects to compensate for the varying levels of diffusivity.

As a supplement to the protocol overview in Table 3, the repository also contains the gradient waveforms used in the FWF sequence (Table 1), the sampling schemes in terms of diffusion directions native to the scanner (.dvs, Table 2), a complete protocol description, and the ElastiX co-registration parameters.

2. Experimental design, materials, and methods

2.1. Hardware and imaging

Imaging was performed on a MAGNETOM 3T Prisma (Siemens Healthcare, Germany) which has a maximum gradient amplitude of 80 mT/m at a slew rate of 200 T/m/s (software version VE11C), and a 20-channel head-coil array. We used a custom pulse sequence based on the diffusion weighted spin-echo (a_ep2d_diff) to support free waveform encoding (FWF, version 1.12a) [5]. Briefly, the FWF sequence replaces the trapezoidal diffusion encoding gradient pulses with waveforms that can be arbitrarily defined by the user (Fig. 3).

We used imaging parameters TR = 3.2 s, TE = 91 ms, FOV = 220 × 220 × 60 mm^3, matrix = 92 × 92 × 25, resolution = 2.5 × 2.5 × 2.5 mm^3, partial-Fourier = 7/8, bandwidth = 1940 Hz/pix, and echo spacing = 0.6 ms. We used interleaved slice excitation, strong fat saturation, in-plane acceleration iPAT = 2 with GRAPPA reconstruction and 30 reference lines. The imaging stack was transversal (axial) and centered on the corpus callosum. The phase encoding was done along the anterior-posterior direction.

A 2D T2-FLAIR was acquired for anatomical reference. Here, we used imaging parameters TR = 5.5 s, TE = 95 ms, FOV = 256 × 256 × 120 mm^3, matrix = 256 × 256 × 50, resolution = 1.0 × 1.0 × 2.4 mm^3, bandwidth = 222 Hz/Px, echo spacing = 8.7 ms, and inversion time 1.9 s. We used interleaved slice excitation, no fat saturation, in-plane acceleration iPAT = 2 with GRAPPA reconstruction and 47 reference lines.

2.2. Gradient waveform optimization

Asymmetric gradient waveforms for tensor-valued diffusion encoding were tailored to the hardware by using the optimization framework by Sjölund et al. [6]. Each waveform was specified as a function of time in discrete steps for three orthogonal axes, denoted

$$\mathbf{g}_{123}(t) = [g_1(t)\ \ g_2(t)\ \ g_3(t)]^{\mathrm{T}} \tag{1}$$

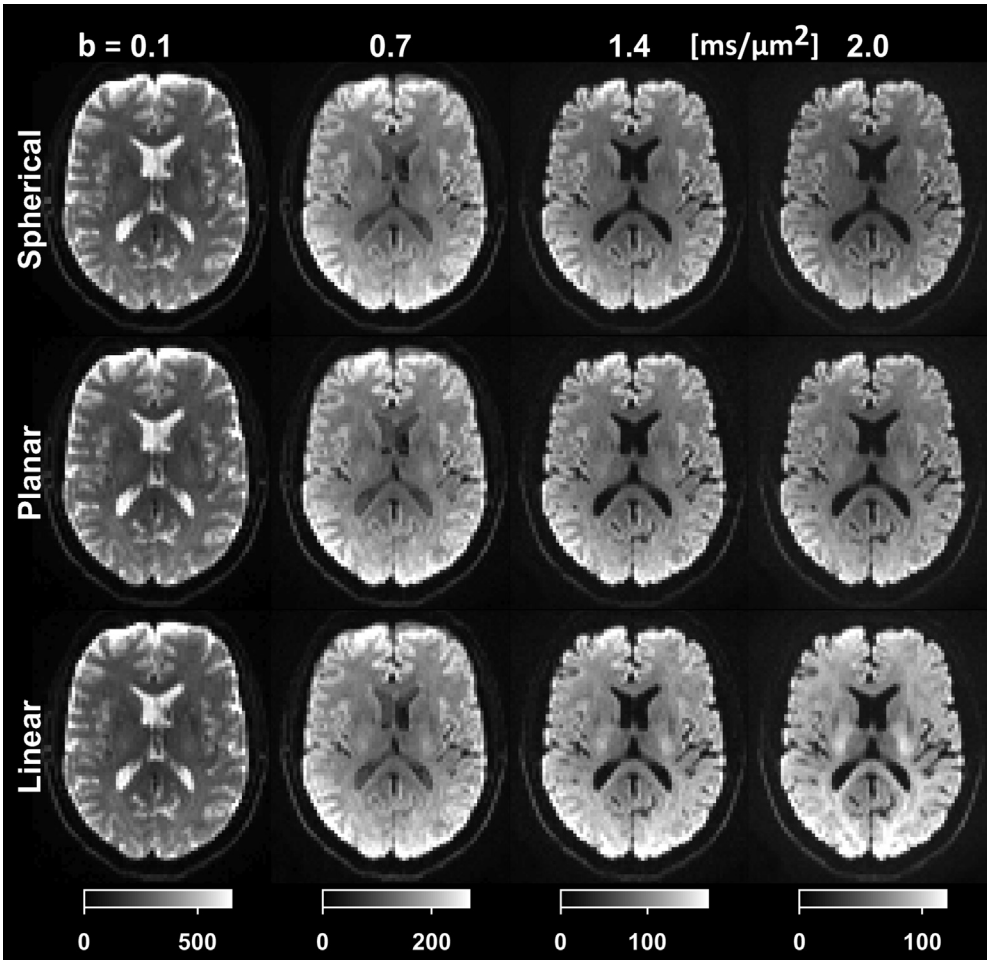

Fig. 2. Signal averaged over rotations for four b-values (columns) and three b-tensor shapes (rows). The color scale is equal within each column but differs within each row. There is an appreciable difference in the spherical and linear encoding at high b-values, where the difference is caused primarily by the presence of anisotropic diffusion [15,21].

Spherical and planar tensor encoding (STE and PTE) were optimized using the Euclidean norm, gradient amplitude limit 80 mT/m, slew rate limit 100 T/m/s, heating coefficient 0.9 and 77 temporal samples. The STE waveform was designed to have its longest diffusion time along g_1 [7]. The waveform used for linear tensor encoding (LTE) was defined as g_1 from STE, making them perfectly matched with respect to the diffusion time spectrum along that direction [7–9]. For all waveforms, the duration of the waveforms before and after the refocusing pulse was 35.67 ms and 30.85 ms separated by 8.02 ms (Fig. 3). Since the waveforms were designed to be asymmetric, they were Maxwell-compensated to alleviate effects of concomitant gradients, as described by Szczepankiewicz et al. [10]. The waveforms are stated in Table 1, and the framework for Maxwell-compensated waveform optimization is available at https://github.com/jsjol/NOW.

The waveform was resampled to match the gradient system raster time (10 μs) by linear interpolation. A balance gradient was used to correct for small timing and interpolation errors so that the zeroth moment of the final gradient waveform was zero [10,11].

Table 1
Gradient waveform samples along the time dimension for linear, planar and spherical encoding. Note that the linear encoding uses only g_1 from the spherical encoding waveform (g_2 and g_3 are zero). The planar encoding was optimized separately and uses only g_2 and g_3 (g_1 is zero). The waveforms are defined in the space that is employed by the gradient system such that the integral is zero only if the second part is multiplied by −1.

Linear and Spherical			Planar	
g_1	g_2	g_3	g_2	g_3
0.0000	0.0000	0.0000	0.0000	0.0000
−0.2005	0.9334	0.3029	−0.7301	0.6840
−0.2050	0.9324	0.3031	−0.7289	0.6853
−0.2146	0.9302	0.3032	−0.7263	0.6880
−0.2313	0.9263	0.3030	−0.7222	0.6924
−0.2589	0.9193	0.3019	−0.7162	0.6986
−0.3059	0.9060	0.2980	−0.7077	0.7072
−0.3892	0.8767	0.2883	−0.6958	0.7189
−0.3850	0.7147	0.3234	−0.6787	0.7350
−0.3687	0.5255	0.3653	−0.6536	0.7575
−0.3509	0.3241	0.4070	−0.6146	0.7894
−0.3323	0.1166	0.4457	−0.5506	0.8353
−0.3136	−0.0906	0.4783	−0.4439	0.8274
−0.2956	−0.2913	0.5019	−0.3217	0.7803
−0.2790	−0.4793	0.5139	−0.1931	0.7293
−0.2642	−0.6491	0.5118	−0.0598	0.6745
−0.2518	−0.7957	0.4939	0.0766	0.6164
−0.2350	−0.8722	0.4329	0.2142	0.5553
−0.2187	−0.9111	0.3541	0.3514	0.4915
−0.2063	−0.9409	0.2747	0.4861	0.4255
−0.1977	−0.9627	0.1933	0.6168	0.3576
−0.1938	−0.9768	0.1080	0.7417	0.2883
−0.1967	−0.9820	0.0159	0.8590	0.2178
−0.2114	−0.9751	−0.0883	0.9672	0.1467
−0.2292	−0.9219	−0.2150	0.9996	0.0406
−0.2299	−0.8091	−0.3561	0.9984	−0.0639
−0.2290	−0.6748	−0.5011	0.9888	−0.1521
−0.2253	−0.5239	−0.6460	0.9749	−0.2247
−0.2178	−0.3620	−0.7868	0.9593	−0.2840
−0.2056	−0.1948	−0.9194	0.9436	−0.3326
−0.1391	−0.0473	−0.9908	0.9283	−0.3730
−0.0476	0.0607	−0.9987	0.9138	−0.4074
0.0215	0.1452	−0.9909	0.8998	−0.4374
0.0725	0.2136	−0.9759	0.8862	−0.4642
0.1114	0.2709	−0.9579	0.8728	−0.4891
0.1426	0.3204	−0.9383	0.8590	−0.5128
0.1690	0.3641	−0.9177	0.8447	−0.5362
0.0000	0.0000	0.0000	0.0000	0.0000
Gradients are off during the refocusing pulse				
0.0000	0.0000	0.0000	0.0000	0.0000
−0.3734	−0.1768	0.9125	−0.6963	0.7184
−0.3825	−0.2310	0.8965	−0.6861	0.7281
−0.3919	−0.2895	0.8752	−0.6748	0.7387
−0.4015	−0.3543	0.8465	−0.6619	0.7502
−0.4108	−0.4290	0.8065	−0.6472	0.7630
−0.4182	−0.5202	0.7469	−0.6301	0.7771
−0.4178	−0.6423	0.6451	−0.6102	0.7928
−0.3855	−0.8173	0.4321	−0.5865	0.8105
−0.3110	−0.9418	0.1401	−0.5578	0.8305
−0.2526	−0.9669	−0.0674	−0.5226	0.8531
−0.2100	−0.9541	−0.2213	−0.4780	0.8789
−0.1766	−0.9227	−0.3474	−0.4199	0.9081
−0.1491	−0.8788	−0.4570	−0.3409	0.9406
−0.1258	−0.8239	−0.5555	−0.2254	0.9747

(*continued on next page*)

Table 1 (*continued*)

Linear and Spherical			Planar	
g_1	g_2	g_3	g_2	g_3
−0.1056	−0.7583	−0.6459	−0.0303	1.0000
−0.0882	−0.6809	−0.7293	0.9549	0.2984
−0.0734	−0.5900	−0.8061	0.9984	0.0635
−0.0615	−0.4830	−0.8753	0.9997	−0.0387
−0.0533	−0.3556	−0.9349	0.9953	−0.1015
−0.0506	−0.2005	−0.9801	0.9899	−0.1448
−0.0575	−0.0019	−1.0000	0.9848	−0.1764
−0.0909	0.2976	−0.9521	0.9802	−0.2004
−0.3027	0.9509	−0.0860	0.9762	−0.2190
−0.2737	0.9610	−0.0692	0.9728	−0.2337
−0.2524	0.9675	−0.0596	0.9699	−0.2452
−0.2364	0.9719	−0.0533	0.9676	−0.2544
−0.2245	0.9749	−0.0490	0.9657	−0.2615
−0.2158	0.9770	−0.0459	0.9642	−0.2669
−0.2097	0.9785	−0.0439	0.9631	−0.2708
−0.2058	0.9794	−0.0426	0.9624	−0.2733
−0.2039	0.9798	−0.0420	0.9621	−0.2745
0.0000	0.0000	0.0000	0.0000	0.0000

2.3. Sampling scheme

The signal was sampled at diffusion encoding strengths $b = [.1, .7, 1.4, 2]$ ms/μm^2. Spherical encoding was performed in 10 rotations for each b-value, and all measurements were repeated five times. Linear and planar encoding was performed in 10, 10, 16, 46 rotations for the same four b-values, respectively. The direction sets were derived from platonic solids (atoms of 6, 10 and 30 directions) so that multiple atoms could be combined with optimal directional coverage of the sphere with no colinear measurements within each shell [12]. Fig. 3 shows the sampling scheme for each shell and shape and all direction sets are defined in Table 2. We also included 13 images without diffusion encoding ($b = 0$).

Each direction vector ($\mathbf{u} = [u_1 \;\; u_2 \;\; u_3]^{\mathrm{T}}$, $|\mathbf{u}| = 1$) defines the target direction of the first axis of the gradient waveform (g_1). The rotated gradient waveform is therefore defined as

$$\mathbf{g}_{\mathrm{xyz}}(t) = \left[g_{\mathrm{x}}(t) \;\; g_{\mathrm{y}}(t) \;\; g_{\mathrm{z}}(t)\right]^{\mathrm{T}} = \mathbf{R}\mathbf{g}_{123}(t) \tag{2}$$

where

$$\mathbf{R} = \begin{bmatrix} u_1 & -u_2\left(1-u_1^2\right)^{\frac{1}{2}}\Big/\left(u_2^2+u_3^2\right)^{\frac{1}{2}} & -u_3\left(1-u_1^2\right)^{\frac{1}{2}}\Big/\left(u_2^2+u_3^2\right)^{\frac{1}{2}} \\ u_2\left(1-u_1^2\right)^{\frac{1}{2}}\Big/\left(u_2^2+u_3^2\right)^{\frac{1}{2}} & u_1-u_3^2(u_1-1)\Big/\left(u_2^2+u_3^2\right) & u_2u_3(u_1-1)\Big/\left(u_2^2+u_3^2\right) \\ u_3\left(1-u_1^2\right)^{\frac{1}{2}}\Big/\left(u_2^2+u_3^2\right)^{\frac{1}{2}} & u_2u_3(u_1-1)\Big/\left(u_2^2+u_3^2\right) & u_1-u_2^2(u_1-1)\Big/\left(u_2^2+u_3^2\right) \end{bmatrix} \tag{3}$$

Note that the waveform amplitude is always scaled such that it yields the requested b-value, and that the timing or duration of the waveforms was never changed.

In total, the signal was sampled 377 times per voxel for a total scan time of approximately 23 min. The design matrix is such that it supports inversion of the q-space trajectory imaging representation (QTI) [12], and all techniques that require equal, or lower, measurement rank, for example diffusional

Table 2
Sets of directions derived from platonic solids [12]. These directions can be arbitrarily combined with no co-linearity and retained isotropic sampling.

u_1	u_2	u_3
6 Directions		
0.0000	0.5257	0.8507
0.0000	0.5257	−0.8507
0.5257	0.8507	0.0000
0.5257	−0.8507	0.0000
0.8507	0.0000	0.5257
−0.8507	0.0000	0.5257
10 Directions		
0.5774	0.5774	0.5774
0.0000	0.9342	0.3568
0.3568	0.0000	0.9342
−0.3568	0.0000	0.9342
−0.5774	0.5774	0.5774
0.0000	0.9342	−0.3568
0.5774	0.5774	−0.5774
0.9342	0.3568	0.0000
0.5774	−0.5774	0.5774
0.9342	−0.3568	0.0000
30 Directions		
0.0000	0.2018	0.9794
0.0000	0.2018	−0.9794
0.2018	0.9794	0.0000
0.2018	−0.9794	0.0000
0.9794	0.0000	0.2018
−0.9794	0.0000	0.2018
0.4035	0.8547	0.3265
0.4035	−0.8547	0.3265
0.4035	0.8547	−0.3265
0.4035	−0.8547	−0.3265
0.8547	0.3265	0.4035
−0.8547	0.3265	0.4035
0.8547	−0.3265	0.4035
−0.8547	−0.3265	0.4035
0.3265	0.4035	0.8547
0.3265	0.4035	−0.8547
−0.3265	0.4035	0.8547
−0.3265	0.4035	−0.8547
0.2018	0.7300	0.6530
0.2018	−0.7300	0.6530
0.2018	0.7300	−0.6530
0.2018	−0.7300	−0.6530
0.7300	0.6530	0.2018
−0.7300	0.6530	0.2018
0.7300	−0.6530	0.2018
−0.7300	−0.6530	0.2018
0.6530	0.2018	0.7300
0.6530	0.2018	−0.7300
−0.6530	0.2018	0.7300
−0.6530	0.2018	−0.7300

variance decomposition (DIVIDE and CODIVIDE) [13–15], diffusion tensor imaging (DTI) [16] and diffusion kurtosis imaging (DKI) [17].

The order of acquisition was permuted so that energy consumption and heating [18], as well as potential system drift, was alleviated [19]; the order of b-values and directions was randomly permuted for each shape. Table 3 shows the acquisition order, and an exact description of the shapes, b-values and directions is available in the metadata.

Table 3
Order of acquisition with different b-tensor shapes. In the case of the water phantom, and oil phantom, the planar encoding was omitted. The time is given in minutes:seconds. The total acquisition time was approximately 23 minutes for the complete protocol.

Shape	Part	Time
Spherical	1/5	2:21
Linear	1/4	1:20
Planar	1/4	1:20
Spherical	2/5	2:21
Linear	2/4	1:20
Planar	2/4	1:20
Spherical	3/5	2:21
Linear	3/4	1:20
Planar	3/4	1:20
Spherical	4/5	2:21
Linear	4/4	1:14
Planar	4/4	1:14
Spherical	5/5	2:21

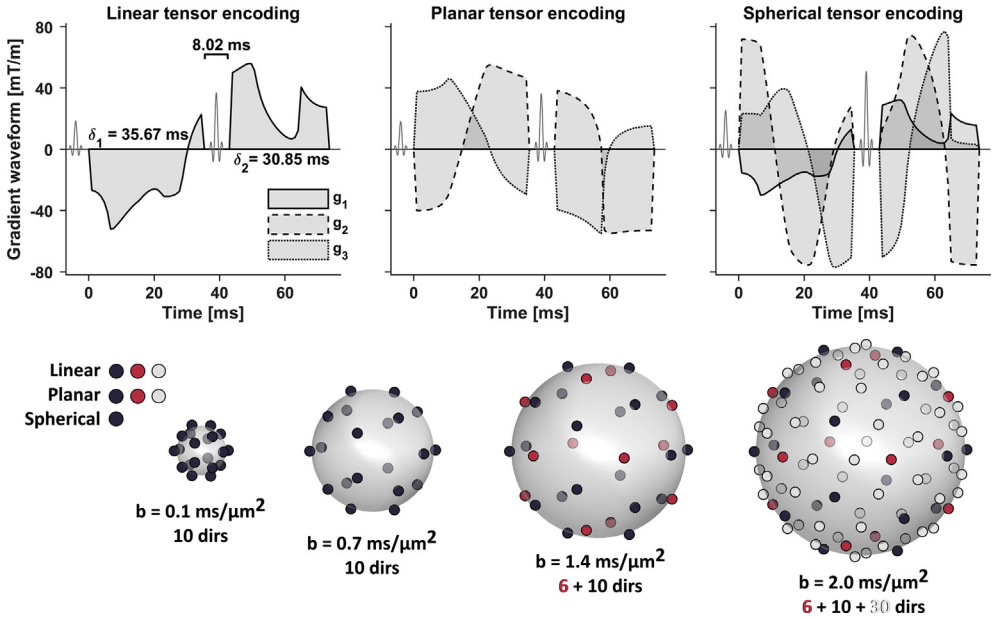

Fig. 3. The top row shows the gradient waveforms used for linear, planar and spherical b-tensor encoding; each waveform is scaled in amplitude to yield $b = 2$ ms/μm^2. The durations of the pulses were identical for all encoding shapes, as shown in the top-left panel. Note that g_1 is the same for both linear and spherical encoding. The bottom row shows the diffusion encoding directions (including antipodal points) of the symmetry axis (g_1).

2.4. Subject and phantoms

In vivo experiments were performed in a single healthy brain (age 53 y, male). The study was approved by the local ethics committee and written consent was given before the study. Identical experiments were also performed in a liquid crystal phantom. The crystals are in a reverse hexagonal phase (HEX), which creates nanometer-scale tubes in which water diffusion is effectively one-dimensional [20]. The liquid crystals therefore exhibit a high microscopic diffusion anisotropy and

variable macroscopic diffusion anisotropy due to variable orientation coherence on the voxel scale. Furthermore, the linear and spherical encoding was performed in water and oil.

As a brief overview, Fig. 1 shows examples of the signal vs b-value in brain, HEX, water and oil, and Fig. 2 shows the signal averaged over direction in an axial slice through the brain for all included b-tensor shapes and b-values.

Acknowledgements

We thank Siemens Healthcare for providing sequence source code and the pulse sequence programming environment. We thank Isaiah Norton for supporting the development of the FWF header tools. This study was supported by the Swedish Research Council, Sweden, grant no. 2016-03443 and 2016-04482; Swedish Foundation for Strategic Research, Sweden, grant no. AM13-0090; NIH, United States, grant no. R01MH074794 and P41EB015902.

Conflict of interest

The authors declare that they have no known competing financial interests or personal relationships that could have appeared to influence the work reported in this paper.

References

[1] W. Newhauser, T. Jones, S. Swerdloff, W. Newhauser, M. Cilia, R. Carver, A. Halloran, R. Zhang, Anonymization of DICOM electronic medical records for radiation therapy, Comput. Biol. Med. 53 (2014) 134–140.
[2] M. Nilsson, F. Szczepankiewicz, B. Lampinen, A. Ahlgren, J.P. De Almeida Martins, S. Lasic, C.F. Westin, D. Topgaard, An open-source framework for analysis of multidimensional diffusion MRI data implemented in MATLAB, in: Proc. Intl. Soc. Mag. Reson. Med., 26, 2018 (Paris, France).
[3] M. Nilsson, F. Szczepankiewicz, D. van Westen, O. Hansson, Extrapolation-based references improve motion and eddy-current correction of high B-value DWI data: application in Parkinson's disease dementia, PLoS One 10 (10) (2015) e0141825.
[4] S. Klein, M. Staring, K. Murphy, M.A. Viergever, J.P. Pluim, elastix: a toolbox for intensity-based medical image registration, IEEE Trans. Med. Imaging 29 (1) (2010) 196–205.
[5] F. Szczepankiewicz, J. Sjölund, F. Ståhlberg, J. Lätt, M. Nilsson, Tensor-valued diffusion encoding for diffusional variance decomposition (DIVIDE): technical feasibility in clinical MRI systems, PLoS One 14 (3) (2019) e0214238.
[6] J. Sjölund, F. Szczepankiewicz, M. Nilsson, D. Topgaard, C.F. Westin, H. Knutsson, Constrained optimization of gradient waveforms for generalized diffusion encoding, J. Magn. Reson. 261 (2015) 157–168.
[7] F. Szczepankiewicz, S. Lasic, C. Nilsson, H. Lundell, C.F. Westin, D. Topgaard, Is spherical diffusion encoding rotation invariant? An investigation of diffusion time dependence in the healthy brain, in: Proc. Int. Soc. Magn. Reson. Med. 27, 2019 (Montreal, Canada).
[8] H. Lundell, M. Nilsson, T.B. Dyrby, G.J. Parker, P. Hubbard, F. Zhou, D. Topgaard, S. Lasic, Microscopic anisotropy with spectrally modulated q-space trajectory encoding, in: Proc. Intl. Soc. Mag. Reson. Med., 25, 2017 (Honolulu, Hawaii).
[9] S. Nørhøj Jespersen, J. Lynge Olesen, A. Ianuş, N. Shemesh, Effects of nongaussian diffusion on "isotropic diffusion" measurements: an ex-vivo micro imaging and simulation study, J. Magn. Reson. 300 (2019) 84–94, https://doi.org/10.1016/j.jmr.2019.01.007.
[10] F. Szczepankiewicz, C.F. Westin, M. Nilsson, Maxwell-compensated Design of Asymmetric Gradient Waveforms for Tensor-Valued Diffusion Encoding, Magn. Reson. Med. (2019).
[11] F. Szczepankiewicz, Imaging diffusional variance by MRI: the role of tensor-valued diffusion encoding and tissue heterogeneity, in: Department of Medical Radiation Physics, Lund University, 2016.
[12] C.F. Westin, H. Knutsson, O. Pasternak, F. Szczepankiewicz, E. Özarslan, D. van Westen, C. Mattisson, M. Bogren, L.J. O'Donnell, M. Kubicki, D. Topgaard, M. Nilsson, Q-space trajectory imaging for multidimensional diffusion MRI of the human brain, Neuroimage 135 (2016) 345–362.
[13] B. Lampinen, F. Szczepankiewicz, J. Martensson, D. van Westen, P.C. Sundgren, M. Nilsson, Neurite density imaging versus imaging of microscopic anisotropy in diffusion MRI: a model comparison using spherical tensor encoding, Neuroimage 147 (2017) 517–531.
[14] F. Szczepankiewicz, D. van Westen, E. Englund, C.F. Westin, F. Stahlberg, J. Latt, P.C. Sundgren, M. Nilsson, The link between diffusion MRI and tumor heterogeneity: mapping cell eccentricity and density by diffusional variance decomposition (DIVIDE), Neuroimage 142 (2016) 522–532.
[15] S. Lasič, F. Szczepankiewicz, S. Eriksson, M. Nilsson, D. Topgaard, Microanisotropy imaging: quantification of microscopic diffusion anisotropy and orientational order parameter by diffusion MRI with magic-angle spinning of the q-vector, Front. Phy. 2 (2014) 11.
[16] P.J. Basser, J. Mattiello, D. Le Bihan, MR diffusion tensor spectroscopy and imaging, Biophys. J. 66 (1) (1994) 259–267.
[17] J.H. Jensen, J.A. Helpern, A. Ramani, H. Lu, K. Kaczynski, Diffusional kurtosis imaging: the quantification of non-Gaussian water diffusion by means of magnetic resonance imaging, Magn. Reson. Med. 53 (6) (2005) 1432–1440.
[18] J. Hutter, M. Nilsson, D. Christiaens, T. Schneider, A.N. Price, J.V. Hajnal, F. Szczepankiewicz, Highly efficient diffusion MRI by slice-interleaved free-waveform imaging (SIFI), in: Proc. Int. Soc. Magn. Reson. Med. 26, 2018 (Paris, France).

[19] S.B. Vos, C.M. Tax, P.R. Luijten, S. Ourselin, A. Leemans, M. Froeling, The importance of correcting for signal drift in diffusion MRI, Magn. Reson. Med. 77 (1) (2017) 285–299.
[20] M. Nilsson, J. Larsson, D. Lundberg, F. Szczepankiewicz, T. Witzel, C.F. Westin, K. Bryskhe, D. Topgaard, Liquid crystal phantom for validation of microscopic diffusion anisotropy measurements on clinical MRI systems, Magn. Reson. Med. 79 (3) (2018) 1817–1828.
[21] F. Szczepankiewicz, S. Lasič, D. van Westen, P.C. Sundgren, E. Englund, C.F. Westin, F. Ståhlberg, J. Lätt, D. Topgaard, M. Nilsson, Quantification of microscopic diffusion anisotropy disentangles effects of orientation dispersion from microstructure: applications in healthy volunteers and in brain tumors, Neuroimage 104 (2015) 241–252.